



Entergy Operations, Inc.
1340 Echelon Parkway
Jackson, MS 39213-8298
Tel 601 368 5758

Michael A. Krupa
Director
Nuclear Safety & Licensing

CNRO-2002-00042

July 24, 2002

U. S. Nuclear Regulatory Commission
Attn: Document Control Desk
Washington, DC 20555-0001

Subject: Entergy Operations, Inc.
Control Rod Drive Mechanism Fracture Mechanics Analysis

Arkansas Nuclear One, Unit 1
Docket No. 50-313
License No. DPR-51

Dear Sir or Madam:

Enclosed please find Engineering Report #EP-01-002-00, *Engineering Report for ASME Code Section XI Analysis of ANO 1 CRDM number 56*. This report provides the analytical evaluation performed for the remaining flaw in control rod drive mechanism (CRDM) penetration #56 in the reactor pressure vessel head penetration at Arkansas Nuclear One, Unit 1 (ANO-1). Entergy Operations, Inc. is providing this report for your information in accordance with the requirements of ASME Boiler and Pressure Vessel Code Section XI Article IWB-3134(b) of the 1992 Edition.

Should you have any questions, please contact Steve Lewis at (601) 368-5444 or Guy Davant at (601) 368-5756.

Very truly yours,

MAK/GHD/baa

Enclosure:

Engineering Report #EP-01-002-00

cc: Mr. C. G. Anderson (ANO) (w/o)
Mr. W. R. Campbell (ECH) (w/o)
Mr. G. A. Williams (ECH) (w/o)

Mr. R. L. Bywater, NRC Senior Resident Inspector (ANO) (w/o)
Mr. E. W. Merschoff, NRC Region IV Regional Administrator (w/o)
Mr. W. D. Reckley, NRR Project Manager (ANO-1) (w/o)

A047

CNRO-2002-00042

ENCLOSURE

ENGINEERING REPORT #EP-01-002-00

Engineering Report for ASME Code Section XI Analysis of ANO 1 CRDM number 56

ENERGY OPERATIONS

Engineering Report

For

ASME Code Section XI Analysis of ANO 1 CRDM number 56

APPLICABLE SITES

ANO Unit 1: GGNS: W-3:
ANO Unit 2: RBS: ECH:

Safety Related: Yes
 No

Prepared by: J. I. Bukharin Date: 11/13/2001
Responsible Engineer

Reviewed by: Fran C. May Date: 11/13/01
Reviewer

Reviewed by: L. S. R. Date: 3/26/02
Supervisor/Reviewer

Approved by: J. R. Hamilton Date: 6/3/02
Responsible CDE Manager
(for multiple site reports only)

RECOMMENDATION FOR APPROVAL

Engineering Report No.: EP-01-002-00

Reviews Completed: Daniel Spond Date: 4-25-02
Preparer

Concurrence: [Signature] Date: 4/29/02
Responsible Manager, ANO

Concurrence: N/A Date: _____
Responsible Manager, GGNS

Concurrence: N/A Date: _____
Responsible Manager, W3

Concurrence: N/A Date: _____
Responsible Manager, RBS

Table of Contents

Section	Title	Page No.
	List of Appendices	3
	List of Tables	4
	List of Figures	4
1.0	Introduction	5
2.0	Characterization of Nozzle and Flaw	5
3.0	Nozzle Stresses	5
4.0	Fracture Mechanics Evaluation	7
5.0	Conclusions	17
6.0	References	18

List of Appendices

Appendix No.	Title	Number of Pages
1	Limit Load Analysis to Determine Allowable Flaw Size	10
2	Fatigue Crack Growth Analysis for Slice I – Pre-repair Condition	15
3	Fatigue Crack Growth Analysis for Slice II – Pre-repair Condition	15
4	Fatigue Crack Growth Analysis for Slice III – Pre-repair Condition	15
5	Fatigue Crack Growth Analysis for Slice IV – Pre-repair Condition	15
6	Fatigue Crack Growth Analysis for Slice I – Post-repair Condition	15
7	Fatigue Crack Growth Analysis for Slice II – Post-repair Condition	15
8	Fatigue Crack Growth Analysis for Slice III – Post-repair Condition	15
9	Fatigue Crack Growth Analysis for Slice IV – Post-repair Condition	15
10	Fatigue Crack Growth Analysis for Slice II – Post-repair Condition for 2,100 cycles	15
11	Technical Review checklist and Comment Sheets	5

List of Tables

Table No.	Title	Page No.
1	Surface Residual Stresses in the Hoop direction	7
2	Results of Fatigue Crack growth Evaluation	16

List of Figures

Figure No.	Title	Page No.
1	Finite Element Analysis stress Contours	6
2	Allowable Flaw Size – Limit Load results Comparison	10
3	Allowable Flaw Size Curves (ASME Section XI & BS-7910)	11
4	Fatigue Crack Growth – Depth {700 cycles}	15
5	Fatigue Crack Growth – Length {700 Cycles}	15
6	Fatigue Crack Growth – Depth {2,100 cycles}	16
7	Comparison of Final Flaw Size with Allowable Flaw Size	17

1.0 Introduction:

The visual inspection of Control Rod Drive Mechanism (CRDM) nozzles, from the outside surface, at Arkansas Nuclear One (ANO) Unit 1 revealed the presence of white deposits at the reactor vessel head penetration (RVHP). Non-destructive examinations (NDE) performed (References 1, 3, and 4) revealed defects in the weld and a part through-wall axial indication in the CRDM nozzle. The axial defect in the nozzle was 0.2 inch deep and extended 1.3 inches above the weld. The repair method utilized was to excavate the weld cavity without disturbing the weld butter of the original weld. The cavity was then repaired utilizing a qualified welding technique. The repair performed on the nozzle weld ensures that the reactor coolant will not wet the remaining flaw. Hence the evaluation of the remaining flaw can be limited to fatigue crack growth owing to normal operating conditions. The evaluation the flaw to ensure continued safe operation in accordance with the requirements of ASME Section XI, IWB-3640 (Reference 6) by fatigue was performed. This report provides the details of the required analysis and the results of the evaluation performed.

2.0 Characterization of Nozzle and Flaw:

The nozzle dimensions, material, and required operational conditions were obtained from Reference 3. The dimension of the flaw remaining in service was:

Flaw Depth: 0.200 inch
Flaw Length: 1.3 inches

3.0 Nozzle Stresses:

The operating stresses for the normal and upset conditions were obtained from Reference 4. The distribution of residual stresses for the region of interest, obtained from the finite element analysis (FEA) contour plots after the repair was performed, is shown in Figure 1, below. This figure shows the circumferential iso-stress contours, which affect an axial flaw. The residual stress magnitude was found to be higher on the inner diameter (ID) surface when compared to the outer diameter (OD) surface.

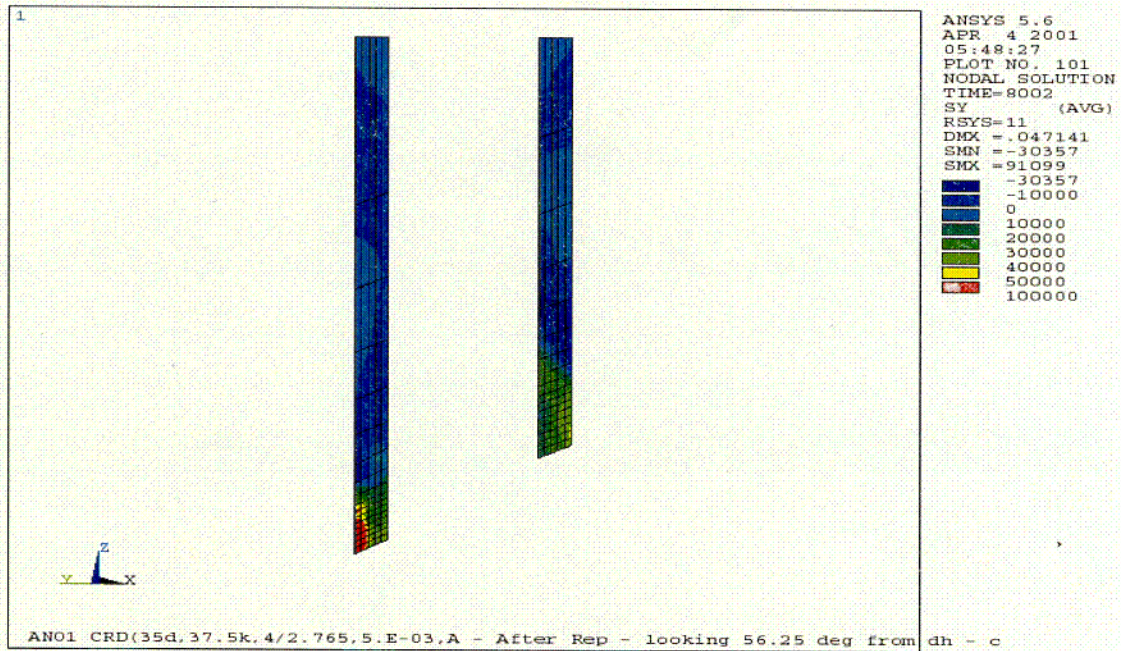


Figure 1: Showing the residual stress contours (hoop stress) in the vicinity of the axial flaw. The finer mesh represents the weld region and the flaw is located just above the weld region on the OD surface. The axial section of the tube, where the repair was performed and where the flaw remains, is on the left side (down hill).

The residual stresses for the as-built and the weld-repaired conditions were obtained from Reference 5. The region where the flaw was located was bounded by four azimuthal slices, which were obtained from detailed FEA. The maximum stress values are located at the 16th, 17th, or 18th row of nodes. The axial location was at the middle of the weld butter plus the rows immediately above the weld. The node numbers in the 5000 series were at the 22.5-degree azimuth and the node numbers in the 6000 series were at the 45-degree azimuth. The four slices chosen represent the zone that bounds the flaw location. The hoop stresses on the OD and ID surfaces were obtained from detailed nodal stress files (Reference 5) and are provided in Table 1 below.

Table 1
Surface Residual Stresses in the Hoop Direction

Slice Location @ Nodes	Surface Hoop Stress {ksi}			
	Asbuilt (pre-repair) Condition		Post-Repair Condition	
	ID	OD	ID	OD
I 61501-61506	43.622	9.372	27.357	-2.977
II 51501-51506	39.397	12.306	33.071	-8.523
III 51601-51606	39.032	8.807	36.073	-13.434
IV 61601-61606	44.203	-0.225	31.340	-16.034

The residual stresses determined by the FEA for both the as-built and the post-repair conditions showed that the magnitude of residual stresses was higher on the ID surface than on the OD surface. The table above clearly demonstrates that after the repair the stress distribution, in the vicinity of the axial crack, was reduced in magnitude. This reduction would only affect the R-ratio for the fatigue crack growth.

4.0 Fracture Mechanics Evaluations:

Limit Load Analysis

The analysis for flaw tolerance for Inconel-600 material at operating temperatures is based on limit load. The first step is to determine the allowable flaw size (depth and length). Based on determining the limiting flaw size, crack growth rate analysis can be performed to determine structural integrity. The fatigue crack growth margin is the difference between the allowable flaw size and the expected final flaw size accounting for design fatigue cycles. Residual stresses are secondary stresses, which only affect the R-ratio in the fatigue analysis and, therefore, are not considered in the limit load analysis. This flaw is captured in the bore of the reactor pressure vessel head and hence limit load-based flaw size is a conservative bounding flaw size.

The critical flaw length, for an axial through wall flaw, was determined to provide a limit for the evaluation. The critical flaw length forms the upper limit on flaw length. This evaluation was based on equation six of Reference 6. The critical flaw length can be defined as:

$$l_{crit} = 2 * \sqrt{\frac{[\frac{\sigma_f}{\sigma_h}]^2 - 1}{1.61} * R_m * t}$$

Where:

- L_{crit} = Critical flaw length (inch)
- σ_f = Material Flow Stress at Operating Temperature (ksi)
- σ_h = Hoop Stress due to Internal Operating Pressure (ksi)
- R_m = Mean Radius of Tube (inch)
- T = Wall Thickness of Tube (inch).

The critical flaw length was determined to be 13.05 inches.

The allowable flaw size based on limit load criteria were determined with a safety factor (SF) of three (SF=3.0). This conservative safety factor was used in the analysis, which is higher than the ASME Section XI safety factor of 2.77. Three methods were compared for the determination of the limit load flaw size. The three methods were as follows:

- 1) The British Standard BS-7910, Amendment 1 (Reference 7)
- 2) ASME Section XI, Appendix "C" (Reference 6)
- 3) EPRI Steam Generator Tube Evaluation (Reference 8)

The material flow stress used in the equations was obtained by using the equation derived for Inconel-600 based on testing steam generator tube materials as demonstrated in Reference 8. The equation for determining flow stress, from Reference 8, is:

$$\sigma_f = 0.58 * \{ \sigma_y + \sigma_u \}$$

Where:

- σ_f = Material Flow Stress at Operating Temperature (ksi)
- σ_y = Material Yield Strength at Operating Temperature (ksi)
- σ_u = Material tensile Strength at Operating Temperature (ksi)

The hoop stresses used in the analyses were defined using both the thin and thick cylinder formulae. The formulation in the British Standard (Reference 7) uses the thick cylinder approximation whereas the ASME code and the EPRI formulation use the thin cylinder approximation. The hoop stress equation for both formulations are presented below.

$$\sigma_{hTK} = P * \frac{R_o^2 + R_i^2}{R_o^2 - R_i^2} \quad \text{Thick Cylinder Formula}$$

$$\sigma_{hTN} = \frac{P * R}{t} \quad \text{Thin Cylinder Formula}$$

Where:

- σ_{hTK} = Hoop Stress using Thick Cylinder formulation(ksi)
- σ_{hTN} = Hoop Stress using Thin Cylinder formulation (ksi)
- R_o = Outer Radius (inch)

R_i = Inner Radius (inch)
 $R = R_o$ for ASME Section XI, and
 $R = R_i$ for ERPRI Methods.

The allowable flaw dimensions using the three methods was determined using the equations defined below.

The British Standard method (Reference 7, equation P 11) defines the flaw dimensions by:

$$d_{BS} = \frac{1 - X}{\frac{1}{M_T} - X} * 100 \quad \text{Equation in British Standard (Reference 7)}$$

Where:

d_{BS} = Part Through Wall Flaw Depth (percent of wall thickness)

$X = \{\sigma_f/SF\}/\{1.2 * \sigma_{hTK}\}$ The factor 1.2 from Reference 7 & SF is the safety factor.

$M_T = \sqrt{\{1 + 1.6 * [l/2]^2 / R_i * t\}}$

Where l is the flaw length and the other variables defined above.

Using the ASME Section XI, Appendix "C" the flaw dimensions can be defined by:

$$d_{ASME} = \frac{1 - Y}{1 - \frac{Y}{M_{ASME}}} * 100 \quad \text{Equation 5 of Reference 6 (Section C-3420)}$$

Where:

d_{ASME} = Part Through Wall Flaw Depth (percent of wall thickness)

$Y = \{\sigma_{hTN} * SF\} / \sigma_f$ SF is safety factor & other variables defined above

$M_{ASME} = \sqrt{\{1 + 1.61 * l^2 / [4 * R_m * t]\}}$ R_m is mean radius & other variables defined above

The EPRI method for flaw depths limited to eighty five percent of wall thickness and the flaw dimension can be defines as (rearrange Equation 4-5 [volume 2], Reference 8):

$$d_{EPRI} = \left[\left(\frac{l + 2 * t}{l} \right) * \left(1 - \frac{SF * \sigma_{hTN}}{\sigma_f} \right) \right] * 100 \quad \text{EPRI equation from Reference 8}$$

Where:

d_{EPRI} = Part Through-Wall Flaw Depth (percent of wall thickness), and other variables defined above.

The EPRI methods presented in Reference 8 provide two other formulations for the determination of flaw dimensions, which are similar to the ASME method. These methods are

for flaw depths greater than eighty five percent of wall thickness. In these methods the flow stress (σ_f) is replaced by tensile strength (σ_u). However the hoop stress equation uses the thin-wall formulation with inside radius (R_i) instead of the outside radius (R_o) that is used in the ASME method.

The five formulations, presented in the preceding equations, were used to determine the flaw dimensions in an iterative manner. The internal pressure utilized in the calculations was 2,500 psi. The tube geometry and initial flaw dimensions used were defined in earlier sections. The material properties used in the analysis were obtained from ASME Code Section II Part D tables U and Y (Reference 9). The calculations were performed using Mathcad. The Mathcad worksheets are provided in Appendix I to this report. The results from the calculations, showing a comparison of the five methods, are presented in Figure 2 below.

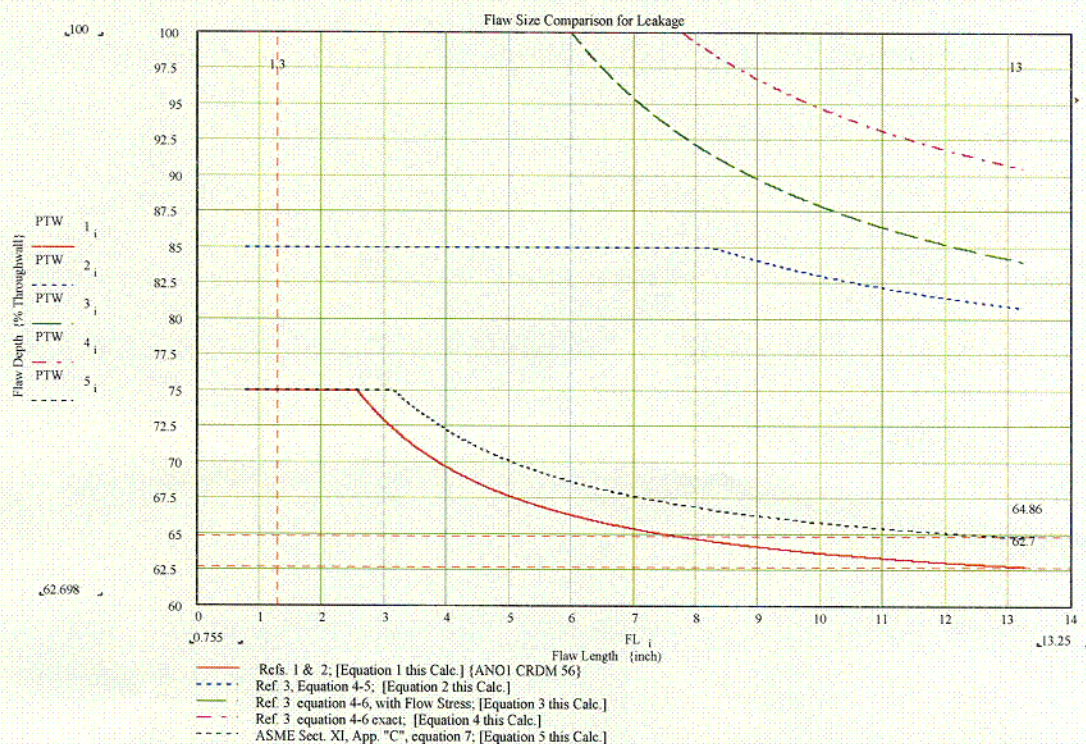


Figure 2: Comparison of allowable flaw size determined by the five methods. The method of the British Standard provides the lowest allowable flaw size.

The results show that the EPRI methods (Reference 8), which were developed for steam generator tubes, show a higher flaw tolerance. The methods used in the ASME Section XI, Appendix "C" (Reference 6) and that in the British standard (Reference 7) provide lower bound flaw sizes. A better comparison between the two lower bound results is presented in Figure 3 below.

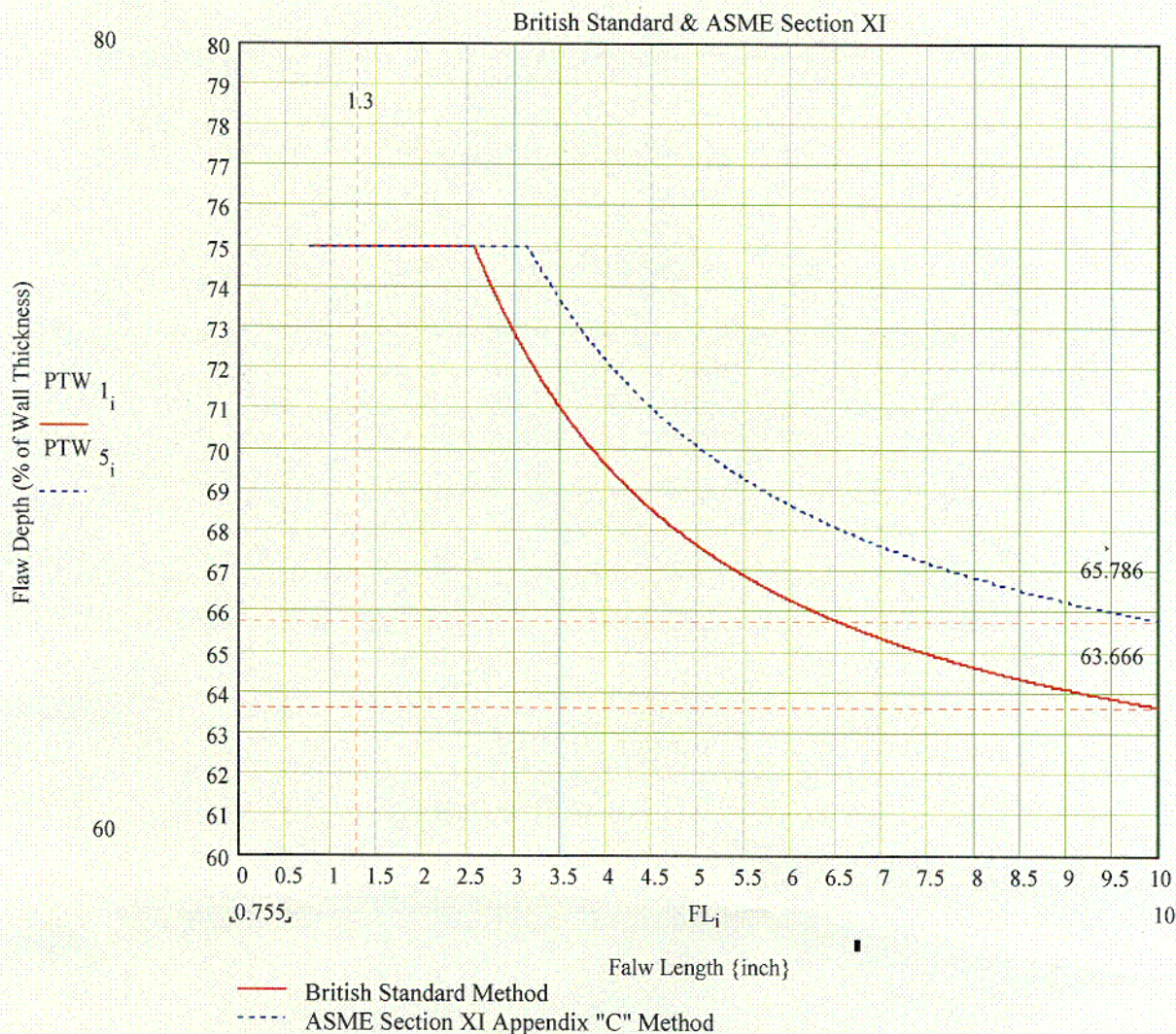


Figure 3: Comparison of flaw size by the British Standard method and the ASME Section XI Appendix "C" method. The British Standard method provides a lower bound solution because of the additional factor of 1.2 applied to the allowable hoop stress.

Figure 3 shows that the British Standard method provides the lowest bound solution owing to the additional reduction of the allowable hoop stress for a thick-wall cylinder. The initial flaw length (1.3 inches) is also shown in this figure. The allowed flaw depth at the initial flaw length is 75 % of wall thickness. However, the measured depth was 31.75 % of wall thickness, which is considerably less than the allowable depth. Figure 3 also shows that the maximum allowable flaw depth extends to a flaw length of about 2.6 inches. This suggests a considerable margin for flaw growth. The weld repair performed assures the eradication of the leak path and hence the remaining flaw will not be subjected to wetting by the reactor coolant. Thus, flaw growth by stress corrosion cracking is mitigated, which implies fatigue due to normal operation as the only viable flaw growth mechanism.

Fatigue Crack Growth Evaluation

The fatigue crack growth evaluation followed the guidance provided in ASME Code Section XI, Appendices A and C. (Reference 6). The stress intensity factor equations of Appendix A (Reference 6) were numerically modeled in the Mathcad worksheet using the formulations provided in Reference 10. The fatigue crack growth formulation from Appendix C (Reference 6) was modeled in the same Mathcad worksheet. Since the stress intensity factor solution in Appendix A (Reference 6) is for a flat plate geometry, a correction factor from Reference 11 (M_p) was applied. This correction factor provides added conservatism (Reference 12). The evaluations were performed with and without the correction factor in order to ascertain the level of conservatism. In the following paragraphs the basic equations used are described. The Mathcad worksheets for the evaluations are presented in Appendices 2 through 9.

The equation for stress intensity factor under the combined action of membrane and bending stresses from Appendix A of Reference 6 is:

$$K_I = \sigma_m * M_m * \left[\sqrt{\frac{\pi * a}{Q}} \right] + \sigma_b * M_b * \left[\sqrt{\frac{\pi * a}{Q}} \right]$$

Where:

K_I = Applied Stress Intensity Factor {ksi $\sqrt{\text{in}}$ }

σ_m & σ_b = Membrane and Bending stresses {ksi} as defined below.

M_m & M_b = Correction Factor for membrane and bending stresses

a = Flaw Depth (inch)

Q = Flaw Shape parameter dependent on flaw geometry and applied stresses

Since the applied stress components are dependent on the flaw depth, the model determines these components in a recursive manner using the formulation provided in Reference 10. The stress components are based on a linearized stress profile between the two surfaces and flaw depth. The basic equations for the stress components are:

$$\sigma_m = \frac{\sigma_a - \sigma_{fs}}{a} * \frac{t}{2} + \sigma_{fs} \quad \text{Membrane stress at flaw tip; and}$$

$$\sigma_b = -\frac{\sigma_a - \sigma_{fs}}{a} * \frac{t}{2} \quad \text{Bending stress at flaw tip}$$

Where:

σ_a = Stress magnitude at Flaw tip {ksi}

σ_{fs} = Stress magnitude at Front Surface (Flaw initiation surface) {ksi}

a & t = Flaw Depth and Wall Thickness respectively {inch}

The correction factors (M_m and M_b), that are dependent on the flaw geometry, are numerically determined following the respective equations provided in Reference 10. The equations for these correction factors are detailed in the Mathcad worksheets provided in the Appendices 2 through 9. In a similar manner the flaw shape parameter “ Q ” was determined using the numerical solution provided in Reference 10. The basic equation for “ Q ”, from Reference 10, is:

$$Q = E_k^2 - 0.212 * \left\{ \frac{\sigma}{\sigma_y} \right\}^2$$

Where:

E_k = Elliptical Integral of the second kind and a function of Flaw Geometry

$\sigma = \sigma_m + \sigma_b$

σ_y = Material Yield Strength at temperature.

The correction factor used to apply the flat plate stress intensity factor solution for a cylinder was obtained from Reference 11. The equation for the correction factor is defined as:

$$M_p = \frac{t - \frac{a}{M}}{t - a} \quad \text{and} \quad M = \left(1 + 1.255 * \frac{l^2}{4 * r * t} - 0.0135 * \frac{l^4}{16 * r^2 * t^2} \right)^{0.5}$$

Where:

M_p = Correction Factor

The equation for fatigue crack growth, obtained from Appendix C of Reference 6, is rearranged to show crack growth increment for a given number of cycles. Thus the total fatigue cycles are divided into a number of blocks and within each block the growth is computed for a set number of cycles. The form of the equation is:

$$CGR_{blk} = CYC_{blk} * C * S * (\Delta K_I)^{3.3}$$

Where:

CGR_{blk} = Crack Growth per Block {inch}

CYC_{blk} = Number of Fatigue Cycles in a Block

C = Scaling parameter to account for temperature effect, defined below

S = Scaling parameter to account for R-ratio (K_{min}/K_{max})

ΔK_I = Stress Intensity Factor Range {ksi $\sqrt{\text{in}}$ }; as defined below

$$C = (10)^{[-10.009 + 8.12 * 10^{-4} * T - 1.13 * 10^{-6} * T^2 + 1.02 * 10^{-9} * T^3]}; \text{ where } T \text{ is the metal temperature.}$$

$S = 1.0$ when $R \leq 0$

$S = 1.0 + 1.8 * R$ when $0 \leq R \leq 0.79$

$$S = -43.35 + 57.97 * R \text{ when } 0.79 \leq R < 1.0$$

$$\Delta K_I = K_{I_{max}} - K_{I_{min}}$$

The parameters in all the equations needed to determine crack growth are dependent on the flaw depth (a). Hence, for each growth increment these parameters would need to be re-calculated. The model to determine fatigue crack growth is designed as a recursive computational scheme to capture the interactive relationships. The computational algorithm is shown in the worksheets in Appendices 2 through 9 to this report.

Four axial slices for which the residual hoop stresses both on the ID and OD surfaces were determined to bound the region of the flaw. The FEAs were performed for the two conditions of interest namely: pre-repair and post repair; hence, eight cases were executed for fatigue crack growth to ensure the determination of maximum growth. The stress intensity factors are computed for both the residual and operating stress conditions. The stress intensity factors for residual and operating stress are summed to obtain the maximum stress intensity factor. The minimum stress intensity factor is calculated using the residual stress alone.

The fatigue crack growth is computed in a recursive manner, since the variables and constants used in the model are a function of the flaw geometry. The initial conditions for flaw depth form the starting conditions. The given and fixed conditions of stresses (residual and operational) on the inside and outside surfaces are prescribed. The operating temperature, material properties, and tube geometry are the fixed inputs. The initial fatigue block, consisting of seven operating cycles, uses the initial conditions to determine the stress components (due to residual stress and operating stresses) and the various constants and factors needed for analysis. The required stress intensity factors are then computed, and using these, the flaw growth for the fatigue block is determined. The numerical algorithm of Reference 10 provides for the determination of stress intensity factors for both the surface and deepest penetration of the flaw. Two parallel computations to accommodate the geometry of a flat plate and that for a cylinder are performed. Likewise, the fatigue crack growth is performed in parallel. The fatigue crack growth is estimated for both the depth and length dimensions. At the end of the recursive cycle the flaw dimensions (depth and length) are updated for the two geometry conditions and the recursive cycle continues the execution. The evaluation is performed for the required seven hundred operating cycles, requiring one hundred fatigue blocks, and the final flaw dimensions are obtained. Figure 4 below shows the results of flaw depth as a function of the number of fatigue cycles, and Figure 5 shows a similar plot for the flaw length. Both figures are for the highest calculated growth for the post-repair residual stress distribution. In these figures the effect of the correction for cylinder geometry appears to be minimal. Both figures show that the increase in the flaw dimension is sufficiently small and are well below the allowable limiting flaw size.

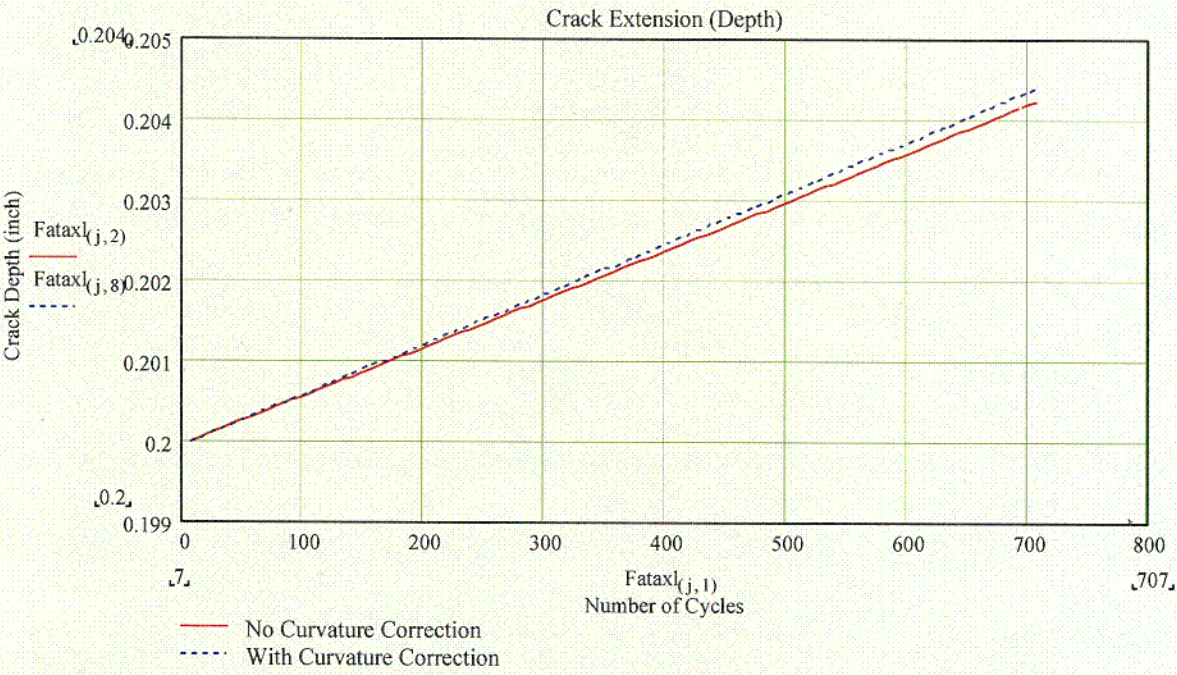


Figure 4: Fatigue crack growth in the depth direction for 700 cycles of operation using the operating stresses and the residual stress after the weld repair

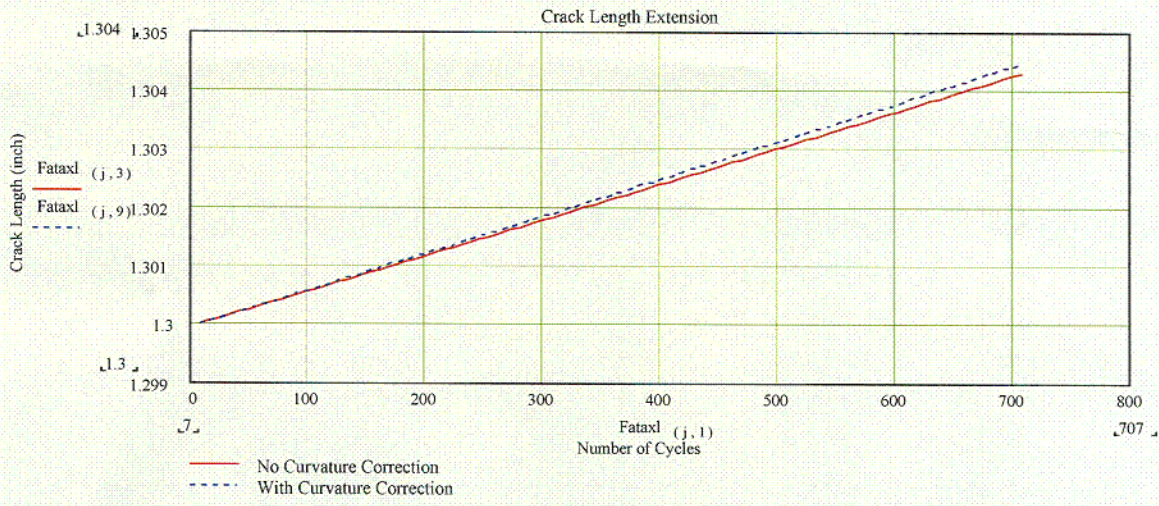


Figure 5: Fatigue crack growth in the length direction for 700 cycles of operation using the operating stresses and the residual stress after the weld repair.

Table 2 provides the final flaw sizes for the eight cases evaluated. The data presented show that the expected flaw growth to be very small and that the final flaw dimensions are well within the acceptable size.

C04

Table 2
Results of Fatigue Crack Growth Evaluation

Case Number	Initial Flaw	Final Flaw Dimension (700 cycles)			
	Dimension	Depth (inch)		Length (inch)	
Residual Stress Distribution Slice Number	Depth / Length (inch)	With Curvature Correction	Without Curvature Correction	With Curvature Correction	Without Curvature Correction
Pre-Repair-I	0.2/1.3	0.20762	0.20732	1.3078	1.3075
Pre-Repair-II	0.2/1.3	0.2069	0.20664	1.3070	1.3067
Pre-Repair-III	0.2/1.3	0.20683	0.20656	1.3069	1.3067
Pre-Repair-IV	0.2/1.3	0.20637	0.20613	1.3065	1.3062
Post-Repair-I	0.2/1.3	0.204194	0.204038	1.30426	1.30410
Post-Repair-II	0.2/1.3	0.204346	0.204184	1.30442	1.30425
Post-Repair-III	0.2/1.3	0.204298	0.204137	1.30437	1.30420
Post Repair-IV	0.2/1.3	0.203818	0.203676	1.30388	1.30374

An additional analysis for expected flaw growth for three times the design operating cycle was performed. The purpose of this analysis was to ascertain the additional expected flaw growth for this extended period of operation. The model used for this analysis was the post-repair case that showed the highest growth (Post-Repair II). The result for this evaluation is presented in Figure 6 and the Mathcad worksheet in Appendix 10.

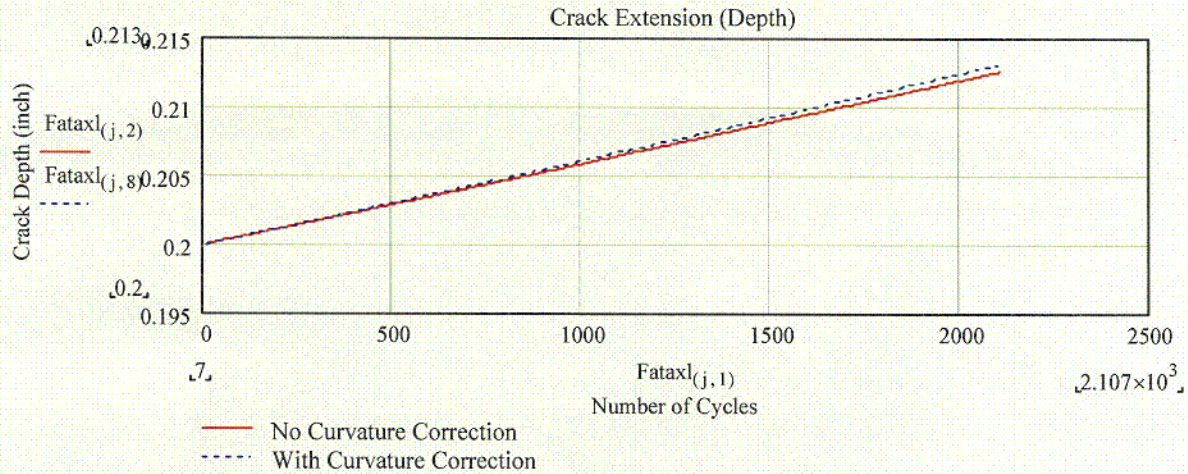


Figure 6: Fatigue crack growth in the depth direction for 2,100 cycles of operation using the operating stresses and the residual stress after the weld repair

5.0 Conclusions:

The critical flaw length for a through-wall axial flaw was determined to be 13.05 inches. The existing flaw is sufficiently smaller and hence net-section collapse failure of the CRDM tube at the flaw location is not plausible. Figure 7 presents the final results of the evaluation. The final flaw size is compared to the allowable flaw size for both the pre-repair and post repair stress distributions. This figure graphically demonstrates the significant margins that exist for the flaw that was left in service.

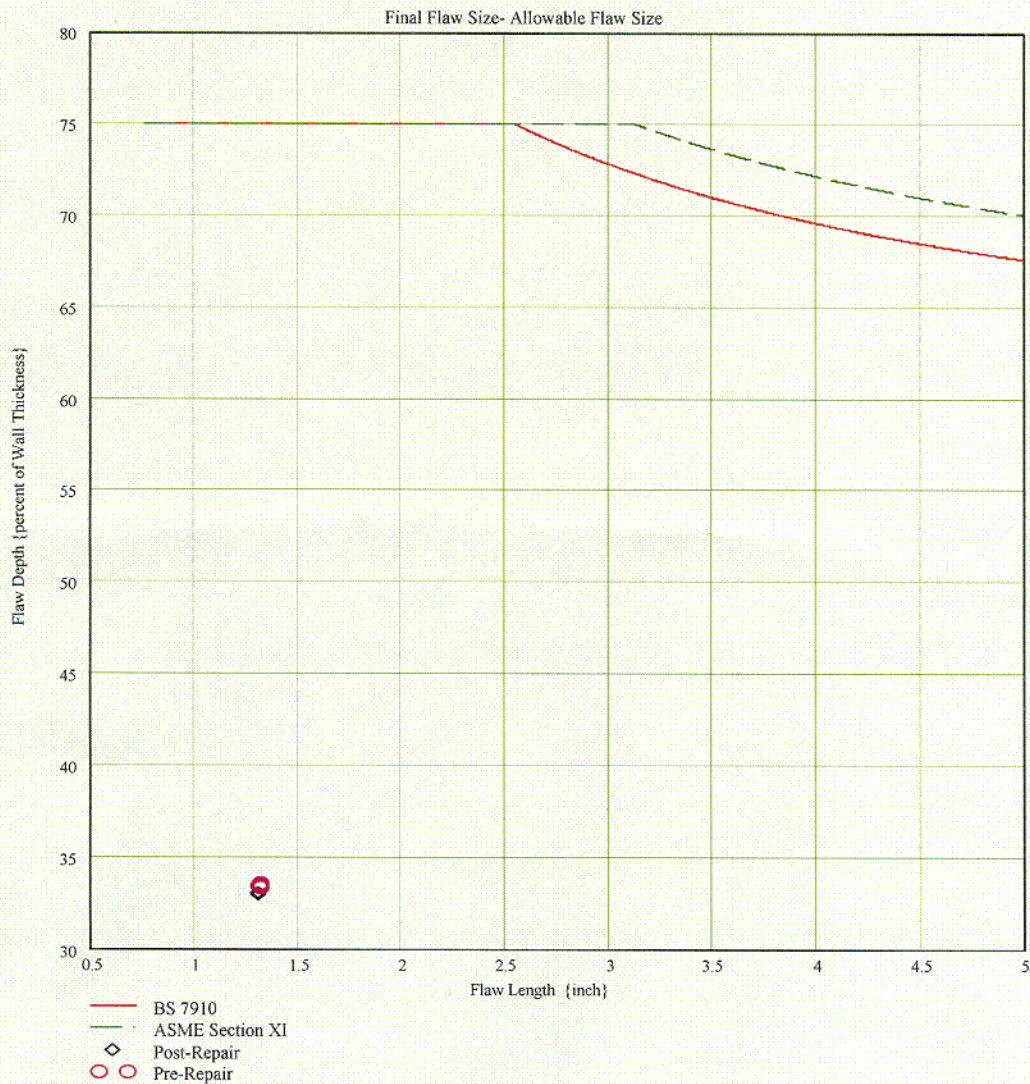


Figure 7: Comparison of final flaw size with the allowable flaw size. Final flaw sizes for both the pre-repair and post-repair stress distributions show considerable margins to the allowable flaw size

COG

The analysis, presented in this report, demonstrates that sufficient margin is available for fatigue crack growth. The fatigue crack growth analysis showed that the final flaw size for the design life of the plant is well within the acceptance criteria prescribed by the ASME Code Section XI, Paragraph IWB-3641.1 of Reference 6.

6.0 References:

- 1) "Entergy Nuclear Southwest Design Input and Descriptions for the ANO Unit 1 CRDM Nozzle Flaw Evaluation", Task # 5. Engineering Programs, Central Engineering; Entergy Operations Inc., March 2001
- 2) Intentionally Left Blank
- 3) "Entergy Nuclear Southwest Design Input and Descriptions for the ANO unit 1 CRDM Nozzle Flaw Evaluation", Task # 9; Engineering Programs, Central Engineering; Entergy Operations Inc., March 2001
- 4) "Entergy Nuclear Southwest Design Input and Descriptions for the ANO unit 1 CRDM Nozzle Flaw Evaluation", Task # 12. Engineering Programs, Central Engineering; Entergy Operations Inc., March 2001
- 5) "Entergy Nuclear Southwest Design Input and Descriptions for the ANO unit 1 CRDM Nozzle Flaw Evaluation", Task # 7; Engineering Programs, Central Engineering; Entergy Operations Inc., March 2001
- 6) ASME Boiler and Pressure Vessel Code, Section XI, 1992 Edition
- 7) "Guide on Methods for Assessing the Acceptability of Flaws in Metallic Structures", Amendment No. 1; Annex P; British Standard BS-7910:1999; British Standards Institute; October 2000
- 8) "Steam Generator Tube Integrity, Volumes 1 and 2", EPRI NP-6865L; Electric Power Research Institute; Palo Alto, CA; June 1991
- 9) ASME Boiler and Pressure Vessel Code, Section II Part D, "Properties", 1992 Edition
- 10) "Computational Method to Perform the Flaw Evaluation Procedure as Specified in the ASME Code, Section XI, Appendix A", EPRI NP-1181, Part 1; Electric Power Research Institute; Palo Alto, CA; September 1979
- 11) "Advanced Fracture Mechanics", Melvin F. Kanninen and Carl H. Popelar; Oxford University Press; New York, NY; 1985
- 12) "Cold Leg Integrity Evaluation", M. E. Mayfield et al; NUREG/CR-1319; February 1980